PLEASE COMPLETE THE PUBLICATION FEE CONSENT FORM BELOW
AND
RETURN TO THE PRODUCTION EDITOR WITH YOUR PROOF CORRECTIONS

Please return this completed form and direct any questions to the Wiley Journal Production Editor at GRLprod@wiley.com.

To order OnlineOpen, you must complete the OnlineOpen order form at:
https://authorservices.wiley.com/bauthor/onlineopen_order.asp
Authors who select OnlineOpen will be charged the standard OnlineOpen fee for your journal, but excess publication fees will still apply, if applicable. **If your paper has generated excess publication fees, please complete and return the form below in addition to completing the OnlineOpen order form online (excess fees are billed separately)**. If you would like to choose OnlineOpen and you have not already submitted your order online, please do so now.

YOUR ARTICLE DETAILS

Journal: *Geophysical Research Letters*

Article: Cabanes, S., Espa, S., Galperin, B., Young, R. M. B., & Read, P. L. (2020). Revealing the intensity of turbulent energy transfer in planetary atmospheres. *Geophysical Research Letters, 47,* e2020GL088685. https://doi.org/10.1029/2020GL088685

OnlineOpen: No **Words:** 3,851 **Tables:** 1 **Figures:** 3 **Total Publishing Units:**12

Journal Base Fee:		$500
Excess Publishing Units:	0@$125	$0
Publication Fee Total:	USD	$500

Please provide the information requested below.
Bill to:

Name: ______________________________

Institution: ______________________________

Address: ______________________________

Phone: ______________________________ Email: ______________________________

Signature: ______________________________ Date: ______________________________

An invoice will be mailed to the address you have provided once your edited article publishes online in its final format. Please include on this publication fee form any information that must be included on the invoice.

Publication Fees and Length Guidelines:
http://publications.agu.org/author-resource-center/

Frequently Asked Billing Questions:
http://onlinelibrary.wiley.com/journal/10.1002/(ISSN)2169-8996/homepage/billing_faqs.pdf

Purchase Order Instructions:
Wiley must be listed as the contractor on purchase orders to prevent delay in processing invoices and payments.

Author Query Form

WILEY

Journal: Geophysical Research Letters

Article: grl61517

Dear Author,

During the copyediting of your manuscript the following queries arose.

Please refer to the query reference call out numbers in the page proofs and respond to each by marking the necessary comments using the PDF annotation tools.

Please remember illegible or unclear comments and corrections may delay publication.

Many thanks for your assistance.

Query No.	Query	Remarks
Q1	AUTHOR: Please verify that the linked ORCID identifiers are correct for each author	
Q2	AUTHOR: Please confirm that given names (Blue) and surnames/family names (Vermilion) have been identified correctly.	
Q3	AUTHOR: Please complete the Publication Fee Consent Form included with your article and return to the Production Editor with your proofs.	
Q4	AUTHOR: Please explain the relevance of the values in red in Table 1.	
Q5	AUTHOR: Please note that your references and their citations have been edited according to APA/AGU style, available at https://www.agu.org/Publish-with-AGU/Publish/Author-Resources/Grammar-Style-Guide	
Q6	AUTHOR: References Arfken and Weber (1999), Boer (1983), Boer and Shepherd (1983), Boffetta and Musacchio (2010), Burgess et al. (2013), Chen et al. (2006), Conrath et al. (1998), Espa et al. (2014), Galperin et al. (2010), Kaspi et al. (2018), Lacorata and Espa (2012) Porco et al. (2003), Porco et al. (2004), Richardson (1926), and Taylor (1992) have not been cited in the text. Please indicate where they should be cited or delete from the reference list.	

Please confirm that the funding sponsor list below was correctly extracted from your article: that it includes all funders and that the text has been matched to the correct FundRef Registry organization names. If a name was not found in the FundRef registry, it may not be the canonical name form, it may be a program name rather than an organization name, or it may be an organization not yet included in FundRef Registry. If you know of another name form or a parent organization name for a “not found” item on this list below, please share that information.

FundRef name	FundRef Organization Name
EC | H2020 | H2020 Priority Excellent Science | H2020 Marie Skłodowska-Curie Actions (MSCA)	EC | H2020 | H2020 Priority Excellent Science | H2020 Marie Skłodowska-Curie Actions

SPi | Journal Code: G R L | Article ID 61517 | Dispatch: 00.00.00 | No. of Pages: 9 | CE: RTL | ME:

AGU ADVANCING EARTH AND SPACE SCIENCE

Geophysical Research Letters

RESEARCH LETTER

10.1029/2020GL088685

Revealing the Intensity of Turbulent Energy Transfer in Planetary Atmospheres

Simon Cabanes[1], Stefania Espa[1], Boris Galperin[2], Roland M. B. Young[3], and Peter L. Read[4]

[1]DICEA, Sapienza Universitá di Roma, Rome, Italy, [2]College of Marine Science, University of South Florida, St. Petersburg, FL, USA, [3]Department of Physics and National Space Science and Technology Center, UAE University, Al Ain, United Arab Emirates, [4]Atmospheric, Oceanic and Planetary Physics, Department of Physics, University of Oxford, Oxford, UK

Key Points:
- We present a new and universal diagnostic to reveal the intensity of turbulent energy transfer in planetary atmospheres
- We show that turbulent energy transfer in Saturn's atmosphere is 4 times less intense than Jupiter's

Supporting Information:
- Supporting Information S1

Correspondence to:
S. Cabanes,
cabanes.simon@gmail.com

Citation:
Cabanes, S., Espa, S., Galperin, B., Young, R. M. B., & Read, P. L. (2020). Revealing the intensity of turbulent energy transfer in planetary atmospheres. *Geophysical Research Letters*, *47*, e2020GL088685. https://doi.org/10.1029/2020GL088685

Received 9 MAY 2020
Accepted 30 OCT 2020

Abstract

Images of the giant planets Jupiter and Saturn show highly turbulent storms and swirling clouds that reflect the intensity of turbulence in their atmospheres. Quantifying planetary turbulence is inaccessible to conventional tools, however, since they require large quantities of spatially and temporally resolved data. Here we show, using experiments, observations, and simulations, that potential vorticity (PV) is a straightforward and universal diagnostic that can be used to estimate turbulent energy transfer in a stably stratified atmosphere. We use the conservation of PV to define a length scale, L_M, representing a typical distance over which PV is mixed by planetary turbulence. L_M increases as the turbulent intensity increases and can be estimated from any latitudinal PV profile. Using this principle, we estimate L_M within Jupiter's and Saturn's tropospheres, showing for the first time that turbulent energy transfer in Saturn's atmosphere is four times less intense than Jupiter's.

1. Introduction

In planetary atmospheres, it is common that the outer atmospheric envelope contains highly turbulent flows powered by solar energy and by a heat flux from within the planet itself (Ingersoll & Pollard, 1982; Vallis, 2006). These thermal energy sources transform into sources of atmospheric motion by driving turbulent eddies whose typical scales do not exceed the Rossby deformation radius, which is typically ~2,500 km for both Jupiter (Young & Read, 2017) and Saturn (Read et al., 2009). It ensures the growth of powerful large scale zonal jets (east-west directed flow with 10,000–20,000 km latitudinal scale) and a host of waves and vortices, among which the small scale forcing is unobservable by direct measurement.

Planetary turbulence is characterized by the nonlinear transfer of energy between different scales of motions in processes known as cascades. Because rotation inhibits vertical motion, turbulent planetary flows are quasi-two-dimensional in the horizontal (i.e., in latitude-longitude) and these cascades transfer energy upscale, from small-scale energy sources up to the large-scale jets, resulting in a kinetic energy spectrum that accords with the well-known Kolmogorov-Kraichnan (KK) law $\Pi_\epsilon^{2/3} n^{-5/3}$ (Kraichnan, 1967). In KK's cascade, the energy transfer rate, Π_ϵ, is crucial for the understanding and quantification of planetary turbulence. It uniquely describes a global estimate of the power continuously exchanged between all scales of motions, that is, between jets, waves, and eddies.

To measure Π_ϵ in planetary flows, a prerequisite is to collect two-dimensional (2-D) horizontal high-resolution velocity maps and then either compute a spectral decomposition or use methods based on structure functions (Arbic et al., 2014). This has been done for several numerical and laboratory experiments that emulate planetary-like flows (Augier & Lindborg, 2013; Cabanes et al., 2020; Read et al., 2018; Schneider & Liu, 2009). Yet for real planets it is only recently that the Cassini mission, by taking high-resolution images of Jupiter's cloud deck, has allowed the first global estimates of the power transferred from small-scale forcing to the jets in a gas giant's atmosphere to be made, yielding $10^{-5} \leq \Pi_\epsilon \leq 10^{-4}$ W kg^{-1} (Galperin et al., 2014; Young & Read, 2017). However, due to a lack of appropriate imaging data, the methods used to make this estimate are impractical for other planets, such as Saturn, Uranus, and Neptune, and recently discovered exoplanets, such as gas dwarf planets and hot Jupiters. Here, we propose a new method that can be used to quantify this power Π_ϵ using only a limited number of readily available measurements.

10.1029/2020GL088685

2. Potential Vorticity and Its Link to Π_ϵ

It has long been known that planetary rotation and stable stratification facilitate the material conservation of potential vorticity (PV) (Pedlosky, 2013). PV is intimately related to the Rossby waves that emerge due to a gradient of planetary vorticity, or the β-effect (Rhines, 1975; Vallis & Maltrud, 1993). $\beta = (2\Omega/R)\cos\theta$, where R is the planetary radius, Ω is the rotation rate, and θ is latitude. In its simplest, incompressible form,

$$PV = (\zeta + 2\Omega)/H, \quad (1)$$

PV combines a dynamical term, the vertical component of relative vorticity ζ, with the intrinsic planetary parameters Ω and the fluid depth H. In planetary atmospheres, turbulent mixing, characterized by the relative vorticity ζ, causes parallel bands of constant PV to emerge, and these bands result in multiple zonal jets (Cho & Polvani, 1996; Dritschel & McIntyre, 2008; Marcus & Lee, 1998; Marcus & Shetty, 2011). PV banding in latitude is thought to result from breaking Rossby waves producing turbulent mixing, which leads to the local homogenization of PV (Dritschel & McIntyre, 2008; Marcus & Shetty, 2011; Phillips, 1956). In this framework, “there is no turbulence without waves” (Galperin et al., 2014), and Rossby waves “conspire” with quasi-2-D turbulence to form jets (Dritschel & McIntyre, 2008). In the present study, we turn this notion on its head, arguing that turbulence generate waves and that PV mixing characterizes the global power Π_ϵ associated with turbulence, including Rossby wave turbulence together with small-scale energetic forcing.

Here, we aim to establish the relationship that exists between PV mixing and the turbulent power Π_ε. To do so, we make use of the analogy drawn by Dritschel and McIntyre (2008) between the banding of constant PV in planetary atmospheres and the layering of constant density in the oceans caused by the turbulent mixing of the vertical density gradient. In the oceans, Thorpe (2005) showed that the vertical density profile is made nonmonotonic by turbulent motion that carries more dense, heavier water above lighter water over a typical distance called the Thorpe scale L_T. The Thorpe scale is estimated by a “sorting algorithm” that converts an unstable, nonmonotonic density profile into a stably stratified profile with density increasing downward (Thorpe, 2005). The Thorpe scale is approximately equal to the Ozmidov scale $L_O = (\Pi_\varepsilon/N^3)^{1/2}$, where Π_ε and N are the rate of turbulent energy transfers to dissipation and the Brunt-Väisälä frequency, respectively. Physically, L_O is a scale at which the turbulent eddy turnover time is equal to the period of internal gravity waves. Numerous experiments and observations show that $0.25L_O \leq L_T \leq 4L_O$ (Thorpe, 2005).

The Thorpe scale can often be easily computed and has become a widely used measure to estimate the rate of turbulent energy transfer to dissipation, Π_ε, in stably stratified flows in the ocean (Gargett & Garner, 2008; Thorpe, 2005) and atmosphere (Clayson & Kantha, 2008; Gavrilov et al., 2005; Kantha & Hocking, 2011), and in computer simulations (Klymak & Legg, 2010). Here we extend the analogy between PV banding in latitude and density layering in the vertical by adapting Thorpe's sorting algorithm to monotonize latitudinal PV profiles. This introduces an analog of the Thorpe scale, which we denote L_M, that leads to an estimate of the turbulent power Π_ϵ in giant planet atmospheres. By applying Thorpe's sorting algorithm to PV monotonization, we explore the analogy between vertical and horizontal turbulent mixing in, respectively, stably stratified and quasi-geostrophic (QG) flows.

To complete our approach, we need an analog for L_O in planetary turbulence. We suggest the length scale $L_\beta \approx (\Pi_\epsilon/\beta^3)^{1/5}$, which compares, by analogy with L_O, the turbulent power Π_ϵ with the strength of the background planetary vorticity β (Vallis & Maltrud, 1993). The question is whether there is a universal relationship between L_M and L_β. To address this, we extend the work of Galperin et al. (2014), in which L_M and L_β were estimated from a limited set of laboratory measurements, by using an unprecedented combination of three independent data sets including laboratory experiments, direct observations of Jupiter atmospheric dynamics, and a numerical model of Saturn's general circulation. This data set allows us to compute both the spectral analysis of 2-D velocity fields, necessary to estimate L_β, and the monotonization of instantaneous PV profiles, necessary to estimate L_M. Then, we make use of our new diagnostic based on PV to give the first estimate of the global turbulent power Π_ϵ from direct observations of Saturn's atmospheric dynamics.

3. Three Independent Sources of Zonal Jet Spectral Diagnostics

The first source used to obtain zonal jet spectral diagnostics is an experimental device that reproduces the conditions required to generate planetary-like zonal jets. The experimental setup is a rotating 70 cm square

10.1029/2020GL088685

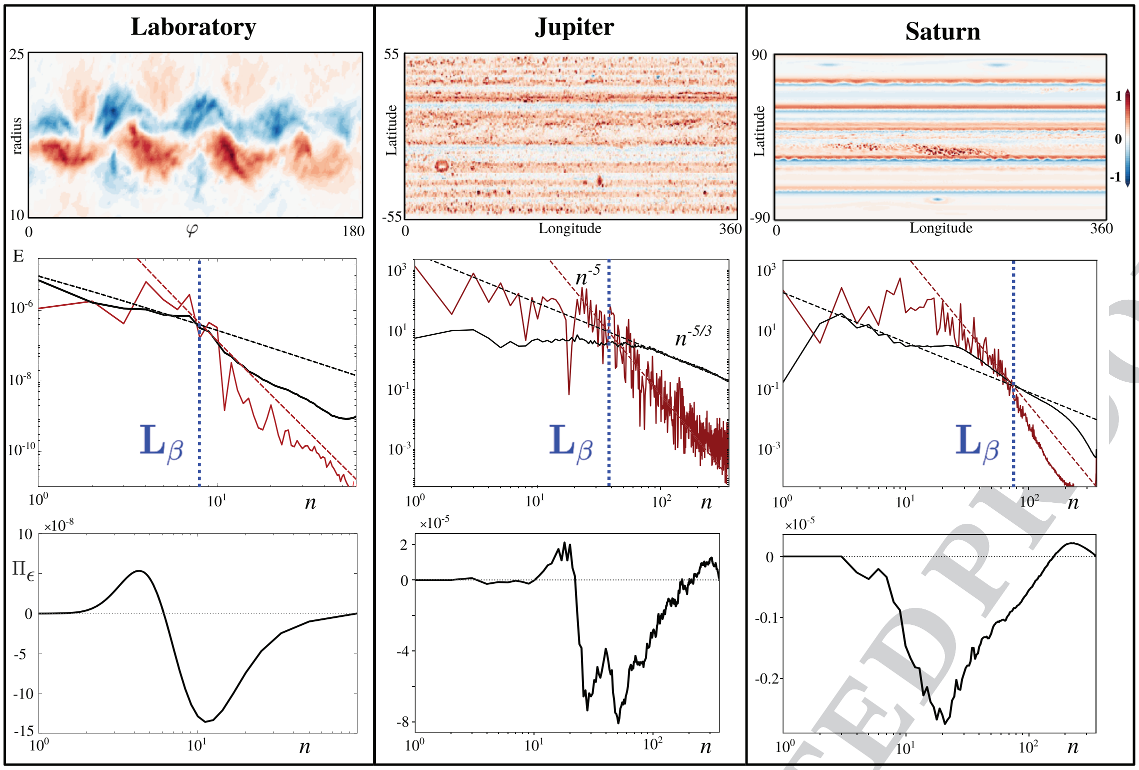

Figure 1. Relative vorticity horizontal maps, energy spectra and energy fluxes. Top panels: Vertical component of the relative vorticity ζ in s^{-1}. The color bar is stretched by a factor of 2 for the 180° westward laboratory jet (3: westward jet 180°), by $\times 10^{-4}$ for the G14g data computed from Cassini images of Jupiter, and by 4×10^{-5} for the Saturn GCM. Middle panels: Zonal energy spectra $E_Z(n)$ (red) and velocity fluctuations energy spectra $E_{KK}(n)$ (black) in $m^{-2}\,s^{-2}$ as a function of nondimensional radial/latitudinal wavenumber n. The dashed lines are theoretical predictions of the zonal energy $E_Z(n) = 0.2\beta^2 n^{-5}$ (red) and the Kolmogorov-Kraichnan (KK) energy $E_{KK}(n) = 6\Pi_\epsilon^{2/3} n^{-5/3}$. In the laboratory $\beta \simeq 53\,m^{-1}\,s^{-1}$, for Jupiter $\beta \simeq 2.5 \times 10^{-12}\,m^{-1}\,s^{-1}$, and for Saturn $\beta \simeq 2.83 \times 10^{-12}\,m^{-1}\,s^{-1}$. Vertical lines are transitional scales L_β that correspond to the intersection of the zonal and KK theoretical spectra. Bottom panels: energy fluxes Π_ϵ in $W\,kg^{-1}$ as a function of nondimensional radial/latitudinal wavenumber n. Positive/negative values of the fluxes refer to downscale/upscale energy transfers. Energy spectra and fluxes are computed from instantaneous velocity maps at steady state and averaged in time (over 58 rotation periods in the laboratory, 4 days for Jupiter observations, and the two last simulated years for Saturn GCM) at each mode n.

tank, filled with 4 cm depth of salt water, which is spun at 29 revolutions per minute. We ran nine independent experiments that generated zonal jets via electromagnetic forcing, using a range of circular magnets placed at the bottom of the tank and centered on the rotating spin axis along an arc of either 90° or 180° (see the experimental device in the supporting information). Experiments differed by the strength and the direction of the forcing, investigating both eastward and westward jets (details are given in supporting information section S1). Experimental measurements of the surface velocities were acquired by recording the tracks of small floating particles from an overhead camera centered in the rotating frame and then by analyzing their paths using a Lagrangian tracking method (Galperin et al., 2016). The 2-D surface velocity maps obtained for each configuration spanned 58 rotation periods (two minutes) at a frequency of 20 Hz (see field maps in Figure 1 and supporting information). F1

The second approach is to use maps of Jupiter's observed cloud-top winds. Two-dimensional horizontal velocity maps were obtained in Galperin et al. (2014) using cloud tracking of high-resolution images taken during Cassini's flyby of Jupiter (see zonal velocity map in Figure 1 and supporting information). In planetary science, PV has long been considered to be fundamentally important when investigating atmospheric dynamics. Therefore, we also make use of zonally averaged Jovian PV profiles computed in Read et al. (2006), at different atmospheric pressure levels (see supporting information figures and section S1). In atmospheric flows assumed to be adiabatic and frictionless, various materially conserved PV diagnostics can be derived. The most fundamental form is the Ertel PV formulation on isentropic surfaces, usually called IPV (Ertel & Rossby, 1949). Under the QG approximation, an alternative form of PV defined on isobaric surfaces is QGPV (Gierasch et al., 2004). Both IPV and QGPV involve thermodynamic terms, in contrast to the barotropic PV in Equation 1, and their exact formulations are detailed in supporting information section S1.

10.1029/2020GL088685

Finally, we use numerical simulations and observations to obtain the same diagnostics for Saturn. Read et al. (2009) repeated the same procedure as for Jupiter and derived IPV and QGPV zonally averaged profiles in latitude at various pressure levels (see all profiles in the supporting information). Unlike Jupiter, however, current observations of Saturn lack the global high-resolution images required to reconstruct 2-D horizontal wind maps. As a result, PV monotonization is the only way we can diagnose the power in Saturn's observed turbulent flow. Using numerical simulations, however, we can obtain 2-D horizontal wind maps. To ensure that our representation of Saturn's dynamics is as realistic as possible, we compute a spectral analysis and PV monotonization using data from a 0.5° resolution, multiannual 3-D numerical simulation obtained by the Saturn Global Climate Model (GCM) described by Spiga et al. (2020) and (Cabanes et al., 2020). This GCM is designed to explore Saturn's tropospheric and stratospheric dynamics with a new icosahedral dynamical core DYNAMICO (Dubos et al., 2015) and realistic radiative transfer (Guerlet et al., 2014). Characteristic 2-D horizontal velocity maps are shown in Figure 1 and supporting information figures. We perform our spectral analysis and PV monotonization within the upper troposphere and lower stratosphere, corresponding to $2 \leq p \leq 650$ hPa .

4. Turbulent Power Computed From the Three Types of Zonal Jets

Figure 1 shows 2-D maps of the instantaneous relative vorticity from a laboratory jet, Jupiter observations, and the Saturn GCM. We compute kinetic energy spectra of the velocity maps by using a Bessel-Fourier decomposition in the cylindrical geometry of the laboratory experiment and a spherical harmonic decomposition in the spherical geometry of Jupiter and Saturn (see supporting information section S1). In order to better characterize the nonlinear dynamics of eddy-eddy interactions, we also compute the fluxes of kinetic energy between different scales of motions, using a filtering procedure in the laboratory and the spherical harmonic decomposition for Jupiter observations and Saturn GCM (see details in supporting information section S1). The spectra and energy fluxes are also shown in Figure 1.

In all cases, we can fit kinetic energy spectra with the theoretical anisotropic zonal flow spectrum:

$$E_Z(n) = C_Z \beta^2 n^{-5} \tag{2}$$

and the KK-law spectrum for velocity fluctuations

$$E_{KK}(n) = C_K \Pi_\epsilon^{2/3} n^{-5/3} \tag{3}$$

where $C_Z = 0.2$ and $C_K = 6$ are taken to be estimated of universal constants and β is estimated at midlatitude (radius) for planetary (laboratory) flow (see in supporting information section S1) (Sukoriansky et al., 2002). The indices n are nondimensional total wavenumbers. For a given n, a typical length scale L is given by $L = \alpha_{mn}/n$ in cylindrical geometry, where α_{mn} are zeros of the Bessel functions and m are zonal indices, and by $L = 2\pi R/n$ when spherical harmonic functions are invoked in planetary geometry, where R is the planetary radius (spectral analysis is detailed in supporting information section S1). The zonal and KK spectra intersect at the scale L_β, which corresponds to the transition scale beyond which planetary vorticity preferentially channels energy into the zonal direction, favoring Rossby waves.

As all other parameters are intrinsic properties of the system (i.e., of the laboratory experiment or the planets), the energy transfer rate Π_ϵ is the only free parameter when setting L_β. To estimate Π_ϵ we fit the KK-law (Equation 3) with the spectrum of velocity fluctuations, shown as dotted and solid black lines in Figure 1. The range of wave numbers where the fit applies appears to be small in the laboratory, well defined for Jupiter observations, and slightly distorted by an energetic bump in the Saturn GCM. The robustness of our approach is ensured by an independent estimate of the energy transfer rate Π_ϵ using energy fluxes. Thus, we fit the KK-law spectra with a value of Π_ϵ that both complies with our estimate from the energy fluxes and a subrange in the spectra that shows a $-(5/3)$ slope. Note that in all cases shown in Figure 1, the wide range of negative energy fluxes show the existence of upscale energy transfers that sustain the jets.

Here, for Jupiter we find $\Pi_\epsilon = 9 \times 10^{-5}$ W kg^{-1} using our fit of the energy spectrum. This estimate is consistent with the energy flux magnitude for Jupiter, which reaches the minimum (negative) value around $\Pi_\epsilon \sim 5 \times 10^{-5}$ W kg^{-1}, and with the range $10^{-5} \leq \Pi_\epsilon \leq 10^{-4}$ W kg^{-1} from Galperin et al. (2014) and Young and Read (2017). For the Saturn GCM, we find $\Pi_\epsilon = 0.13 \times 10^{-5}$ W kg^{-1}, consistent with the minimum (negative) value of the energy flux $\Pi_\epsilon \sim 0.25 \times 10^{-5}$ W kg^{-1} (see also Cabanes et al., 2020). This estimate of Π_ϵ is

10.1029/2020GL088685

Table 1
Summary of the Measured Diagnostics in All Data Sets

	Data set	Π_ϵ (W kg^{-1})	L_M (cm) or (km)	L_β (cm or km)	L_M/L_β
Laboratory	1: Westward jet 90°	$(2.1–0.7) \times 10^{-8}$	1.38 (±0.7)	2.04 (±0.3)	0.68 (±0.36)
	2: Westward jet 90°	$(11–13) \times 10^{-8}$	1.80 (±0.9)	3.14 (±0.1)	0.57 (±0.29)
	3: Westward jet 90°	$(29–7.0) \times 10^{-8}$	1.90 (±1.1)	3.26 (±0.6)	0.58 (±0.36)
	1: Eastward jet 90°	$(2.1–1.5) \times 10^{-8}$	1.00 (±0.7)	2.15 (± 0.1)	0.46 (±0.32)
	2: Eastward jet 90°	$(11–12) \times 10^{-8}$	1.87 (±1.0)	3.12 (±0.04)	0.60 (±0.32)
	3: Eastward jet 90°	$(21–40) \times 10^{-8}$	2.40 (±1.0)	3.73 (±0.3)	0.64 (±0.27)
	1: Westward jet 180°	$(2.0–0.6) \times 10^{-8}$	1.25 (±0.7)	2.00 (±0.3)	0.62 (±0.36)
	2: Westward jet 180°	$(8.0–3.0) \times 10^{-8}$	1.64 (±1.0)	2.65 (±0.4)	0.62 (±0.38)
	3: Westward jet 180°	$(20–14) \times 10^{-8}$	1.89 (±1.1)	3.34 (±0.1)	0.56 (±0.33)
Jupiter	2-D Cassini maps	$(9–5) \times 10^{-5}$	5,200 (±2,500)	11,600 (±970)	0.45 (±0.22)
	QGPV: CIRS - IRIS	$\sim(0.3–2) \times 10^{-5}$	3,500–5,000	6,000–8,600	0.58
	IPV: CIRS - IRIS	$\sim(0.6–3) \times 10^{-5}$	4,200–5,600	7,200–9,700	0.58
Saturn	Global Climate Model	$(0.13–0.25) \times 10^{-5}$	3,400 (±2,000)	5,200 (±490)	0.64 (±0.38)
	QGPV	$\sim 0.9 \times 10^{-5}$	4,200	7,200	0.58
	IPV	$\sim 0.5 \times 10^{-5}$	3,700	6,400	0.58

Note. Details for each laboratoryconfiguration are listed in supporting information Table S1. The turbulent power Π_ϵ reported in this table and used to estimate L_β are obtained using a fit of the velocity fluctuations spectra and spectral energy fluxes and are in W kg^{-1}. Typical length scales L_M and L_β are in cm in the laboratory and in km for Jupiter and Saturn, respectively. Estimates in red are obtained using the averaged relationship with its averaged standard deviation $L_M/L_\beta \simeq 0.58 \pm 0.3$. In the laboratory one can also consider the standard error of the mean for the relationship $L_M/L_\beta \simeq 0.59 \pm 0.02$. Typical length scales and the ratio L_M/L_β are reported with their standard deviation values in brackets, ±0.3 is the averaged value over the three data sets, and ±0.02 is the standard error of the mean over the nine experimental runs in the laboratory. For QGPV and IPV measurements the standard deviation is ±2,000 km (note reported in the table). The averaging procedures and the computation of the standard deviations are detailed in supporting information section S1.

much lower than for Jupiter but is likely to be underestimated as the model does not include several important energy sources such as moist convection and turbulent instabilities caused by an internal heat flux. Numerical approximations also damp the global energy budget by implementing an artificial hyperdiffusivity that compensates for unresolved subgrid-scale processes and substantially reduces turbulent mixing at the smallest scales (Cabanes et al., 2020). In the laboratory, the westward jet presented in Figure 1 has an energy transfer rate $\Pi_\epsilon = 20 \times 10^{-8}$ W kg^{-1}, consistent with the minimum (negative) value of the energy flux $\Pi_\epsilon \sim 14 \times 10^{-8}$ W kg^{-1}. In the data set of laboratory experiments, the energy transfer rate values for Π_ϵ vary between $(2–30) \times 10^{-8}$ W kg^{-1} using our fit of the energy spectra and between $(0.6–40) \times 10^{-8}$ W kg^{-1} using the minimum value from spectral energy fluxes (see supporting information figures for additional spectra and energy fluxes). It has been established elsewhere that structure function analyses also confirm our estimate of the energy transfer rate Π_ϵ and corroborate the robustness of our estimates of L_β (Galperin et al., 2016, for laboratory jets, and Young & Read, 2017, for Jupiter). For all data sets, we compute L_β using the energy transfer rates Π_ϵ estimated from both the energy fluxes and our fit of the energy spectra. All values of Π_ϵ are reported in Table 1 together with the averaged estimate of L_β and its standard deviation. In all three cases, laboratory, Jupiter, and Saturn, our estimate of the theoretical scale L_β successfully fits the intersection of the zonal and residual spectra.

Figure 2 displays sample profiles of instantaneous mean zonal velocity, their corresponding PV profiles, and their associated monotonized PV profiles computed using a Thorpe-like sorting algorithm, for all three cases. In all profiles, PV is strongly mixed and homogenized on jet flanks by the turbulent eddies. This reshapes the large-scale PV distribution into a staircase, causing velocity profiles to sharpen. According to the classical understanding, jets form into bands of monotonic PV, as claimed by Marcus and Lee (1998), Dritschel and McIntyre (2008), and Marcus and Shetty (2011). However, we clearly show Figure 2 that staircase features are actually strongly nonmonotonic (also see supporting information figures of PV profiles for experiments, observations, and simulation). We suggest that this nonmonotonicity contains information

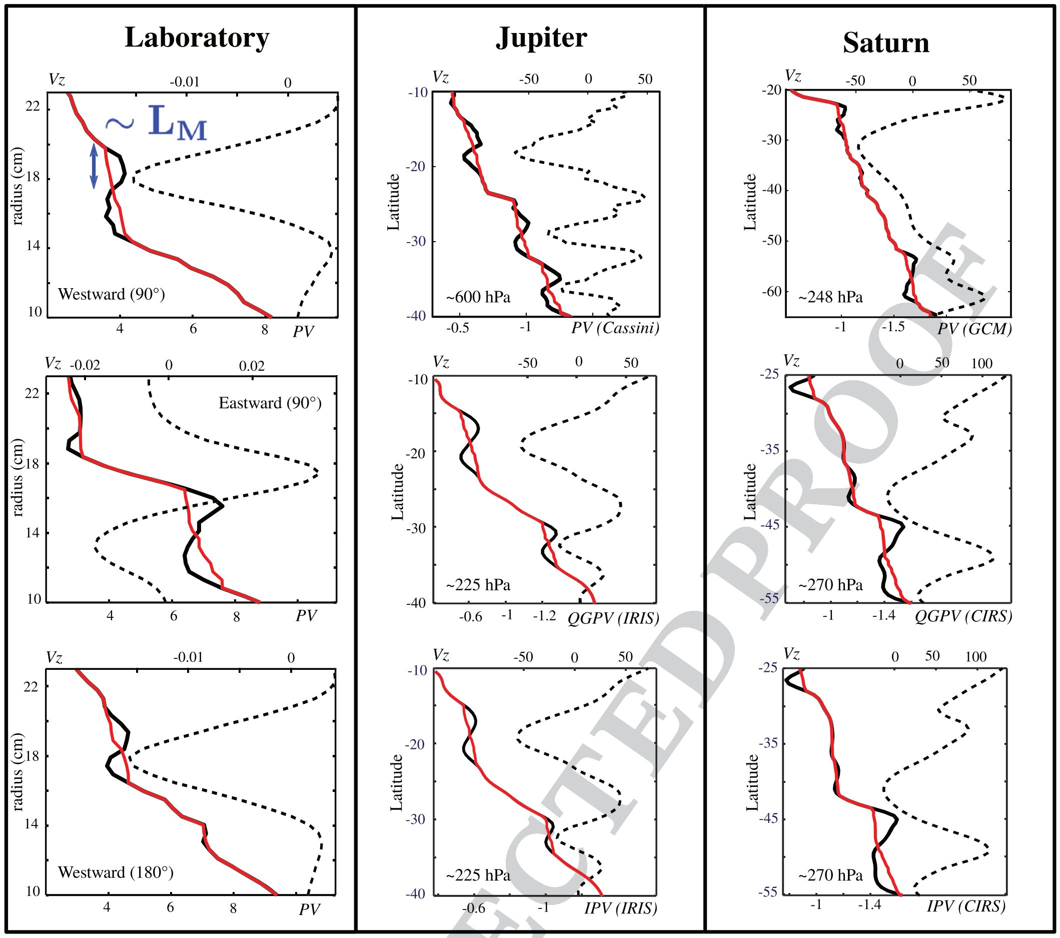

Figure 2. Profiles of the zonal velocity and the corresponding potential vorticity. Instantaneous zonally averaged zonal velocity profiles are dashed lines in m s^{-1}. Instantaneous nondimensional (normalized by the rotation rate Ω and the mean layer depth) potential vorticity (PV), isentropic potential vorticity (IPV), and quasi-geostrophic potential vorticity (QGPV) profiles are solid black lines. In blue, an indicative typical scale L_M. The names in brackets indicate where the data come from. IRIS stands for InfraRed Interferometric Spectrometer of Voyager spacecraft, and CIRS stands for Cassini Composite InfraRed Spectrometer that delivered thermal measurements. Monotonized potential vorticity (using a sorting algorithm, see supporting information section~S1) are in red solid lines. Atmospheric pressure levels at which PV is measured are labeled in each panel.

about rich dynamics involving energy exchanges between jets, Rossby waves, and turbulent eddies and that the (average) magnitude of these energy exchanges can be summarized in turbulent power Π_ϵ.

PV profiles are nonmonotonic over a typical length scale L_M, as indicated in Figure 2. We suggest that L_M can be interpreted as the latitudinal distance over which PV is transported by turbulent mixing but which is then limited by planetary vorticity gradients from converting turbulent eddies into zonal jets. L_M is nearly equivalent to L_β, which defines the scale above which the jets become the most energetic scale of motions, that is, where $E_Z > E_{KK}$.

To extract the length scales L_M, we monotonize the latitudinal PV, IPV, and QGPV profiles using the sorting algorithm. To obtain an overall characterization of these turbulent processes, we consider the root-mean-square (RMS) and the standard deviation for L_M over all longitudes, latitudes, and times (the monotonization and averaging procedure are described in supporting information section S1). These scales L_M are summarized in Table 1. They correspond to 1–2 $\pm$ 0.9 cm in the laboratory and to thousands of kilometers in the gas giants: ~4,500 km for Jupiter and ~3,800 km for Saturn and with standard deviations of ±2,000 km. Overall, the relationship between L_M and L_β can be summarized as $L_M/L_\beta \simeq 0.58 \pm 0.3$; L_M is an intermediate length scale between the small-scale energy sources and L_β. This relationship holds

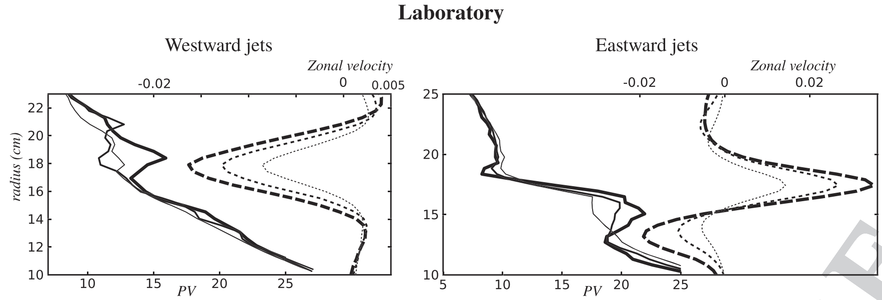

Figure 3. Laboratory potential vorticity and averaged zonal velocity. PV profiles are thick lines in units of $\times 10^{-4}\ \mathrm{s}^{-1}$, and zonal velocity profiles are dashed lines in $\mathrm{m\,s}^{-1}$. The left (right) panels are three westward (eastward) jets for a 180° (90°) arc of magnets and for three different forcing currents $I = 2$, 4, and 6 A, indicated by the lines' thickness and referenced as Data Sets 1, 2, and 3 in Table 1. Increasing thickness means increasing current intensity, hence increasing forcing strength and nonmonotonicity of the PV profiles.

reasonably well across all three data sets (laboratory, Jupiter, and Saturn), but the uncertainty is calling for further analysis of a local estimate, that is, at smaller scale, rather than a global estimate of the turbulent energy transfers Π_ϵ.

From our laboratory experiments, we show in Figure 3 that, as Π_ϵ increases, the nonmonotonicity of the PV profiles also increases. This confirms the existence of a common trend between L_M and L_β and supports our use of PV monotonization to characterize the turbulent power in the flow. We can also compute the standard error of the mean over the nine experimental runs, leading to the ratio with its uncertainty $L_M/L_\beta \simeq 0.59 \pm 0.02$, instead of the mean of the standard deviation, leading to the previous ratio $L_M/L_\beta \simeq 0.58 \pm 0.3$.

Here, one has to consider that the reproducibility of the ratio over the nine experimental runs reduces the uncertainty in the particular configuration of the laboratory. We note, however, that IPV and QGPV diagnostics for Jupiter lead to values of L_M (thus values of Π_ϵ) that are slightly lower than those obtained using PV profiles from the Cassini 2-D horizontal vorticity fields (Table 1). This is expected, as IPV and QGPV are derived from zonally averaged velocity and temperature measurements, in which the averaging procedure likely reduces the turbulent signature in the PV profiles. Finally, the Saturn GCM value for L_M is also low, due to numerical limitations when simulating highly turbulent flow, as described above.

5. Implications for Planetary Turbulence

We have demonstrated that, for rotating turbulence with a β effect and an upscale energy cascade, there exists a length scale L_M which provides an overall picture of the dynamics by allowing for a straightforward estimate of the intensity of turbulent energy transfer Π_ϵ. This estimate relies on the relationship $L_M/L_\beta \simeq 0.58 \pm 0.3$, which we argue is universal by the unprecedented set of data to which it applies: laboratory experiments, GCMs, and direct observations of two different planetary atmospheres. Also, the independent procedures used to estimate L_β (i.e., using a fit of the energy spectra and spectral energy fluxes) argue for the universality of the relationship L_M/L_β. L_M can be computed easily just from a zonal mean zonal velocity profile, the planetary rotation rate, and an estimate of the atmospheric scale height, which is much more amenable than the 2-D horizontal wind maps required hitherto.

With Π_ϵ, one can retrieve the global distribution of kinetic energy, from small-scale sources up to the jet scale, by using the theoretical energy spectra $E_Z(n)$ and $E_{KK}(n)$. In flows with spatially inhomogeneous energy sources, this method has the power to trace back the turbulent energetic sources in planetary atmospheres, which is otherwise impractical. The theory applies in several natural settings, such as atmospheres of the gas giants and of exoplanets as well as the Earth's oceans.

For Saturn, where Π_ϵ has not yet been measured, we can use L_M to predict its value. By monotonizing IPV and QGPV profiles from Read et al. (2009) and then using $L_M/L_\beta \simeq 0.56 \pm 0.3$, we find for Saturn's atmosphere a turbulent power of $0.5 \times 10^{-5} \leq \Pi_\epsilon \leq 0.9 \times 10^{-5}\ \mathrm{W\,kg^{-1}}$, with an uncertainty of 1 order of magnitude that corresponds to $L_M \simeq 3{,}700$ to 4,200 ($\pm$2,000) km (red values in Table 1). As discussed above, this estimate of Π_ϵ is likely to be an underestimate based on the averaged QGPV and IPV from which it is estimated. Also, measuring Π_ϵ offers the opportunity to estimate the latitudinal eddy diffusivity coefficient, K_θ, within Jupiter's and Saturn's atmospheres. K_θ reflects the turbulent mixing in the meridional direction (along the latitude), and we find $K_\theta \sim (1-7) \times 10^6$ m^2 s^{-1} for Jupiter and ∼(1.1–1.6) × 10^6 m^2 s^{-1} for Saturn (see supporting information section S1). Using these eddy diffusivity coefficients with a one-dimensional diffusion equation, one can predict the meridional dispersion of any natural conservative tracer in these atmospheres. Our results are in good agreement with the values obtained by Friedson et al. (1999) from the observation of the meridional spread of Shoemaker-Levy 9 comets' debris for Jupiter and dispersion of gases for Saturn Friedson and Moses (2012). We conclude that Saturn's atmosphere is likely to have an intensity of turbulent energy transfer (Π_ϵ) and thus an intensity of turbulent mixing (K_θ), 2 to 4 times less than Jupiter's. We can speculate that part of this difference simply reflects the fact that Saturn is nearly twice as far from the sun as Jupiter and hence receives a quarter of the solar energy input. Nonetheless, our estimate of Saturn's turbulent power carries an uncertainty that largely exceeds a factor 4 (with a 1 order of magnitude uncertainty). Such uncertainty likely reflects that the global atmospheric dynamics is summarized in a single value of energy transfer rate Π_ϵ while the parameter β itself is latitudinally dependent. However, this is the first estimate of Saturn's turbulent power using the available data, which was not designed for such an analysis, and this study paves the way for future data collection from planetary atmospheres.

Because it is universal, the relationship between L_M and L_β can be used to diagnose the intensity of turbulent energy transfer (as well as turbulent mixing) in many other natural settings for which PV is conserved, such as the Earth's ocean and newly discovered exoplanets.

Data Availability Statement

Data sets related to this article can be found at https://doi.org/10.5281/zenodo.3634814, an open-source online data repository hosted at Zenodo (Zenodo.org).

Acknowledgments
This project has received funding from the European Union's Horizon 2020 research and innovation programme under the Marie Skodowska-Curie grant agreement N° 797012. B. G. was partially supported by the NASA/NOAA Ocean Surface Topography Science Team (Grant Nos. 2500171500 and 2500171600) and by a University of South Florida Nexus Initiative (UNI) Award (No. RP0101). R. M. B. Y. and P. L. R. acknowledge funding support from the UK Science and Technology Facilities Council (STFC) under Grants ST/K502236/1, ST/K00106X/1, and ST/I001948/1.

References

Arbic, B. K., Müller, M., Richman, J. G., Shriver, J. F., Morten, A. J., Scott, R. B., et al. (2014). Geostrophic turbulence in the frequency-wavenumber domain: Eddy-driven low-frequency variability. *Journal of Physical Oceanography*, *44*(8), 2050–2069.

Arfken, G. B., & Weber, H. J. (1999). *Mathematical methods for physicists*: AAPT.

Augier, P., & Lindborg, E. (2013). A new formulation of the spectral energy budget of the atmosphere, with application to two high-resolution general circulation models. *Journal of the Atmospheric Sciences*, *70*(7), 2293–2308.

Boer, G. J. (1983). Homogeneous and isotropic turbulence on the sphere. *Journal of the Atmospheric Sciences*, *40*(1), 154–163.

Boer, G. J., & Shepherd, T. (1983). Large-scale two-dimensional turbulence in the atmosphere. *Journal of the Atmospheric Sciences*, *40*(1), 164–184.

Boffetta, G., & Musacchio, S. (2010). Evidence for the double cascade scenario in two-dimensional turbulence. *Physical Review E*, *82*(1), 016307.

Burgess, B. H., Erler, A. R., & Shepherd, T. G. (2013). The troposphere-to-stratosphere transition in kinetic energy spectra and nonlinear spectral fluxes as seen in ECMWF analyses. *Journal of the Atmospheric Sciences*, *70*(2), 669–687.

Cabanes, S., Spiga, A., & Young, R. M. B. (2020). Global climate modeling of Saturn's atmosphere. Part III: Global statistical picture of zonostrophic turbulence in high-resolution 3D-turbulent simulations. *Icarus*, *345*, 113705. https://doi.org/10.1016/j.icarus.2020.113705

Chen, S., Ecke, R. E., Eyink, G. L., Rivera, M., Wan, M., & Xiao, Z. (2006). Physical mechanism of the two-dimensional inverse energy cascade. *Physical Review Letters*, *96*(8), 084502.

Cho, J. Y. K., & Polvani, L. M. (1996). The morphogenesis of bands and zonal winds in the atmospheres on the giant outer planets. *Science*, *273*(5273), 335.

Clayson, C. A., & Kantha, L. (2008). On turbulence and mixing in the free atmosphere inferred from high-resolution soundings. *Journal of Atmospheric and Oceanic Technology*, *25*(6), 833–852.

Conrath, B. J., Gierasch, P. J., & Ustinov, E. A. (1998). Thermal structure and para hydrogen fraction on the outer planets from Voyager IRIS measurements. *Icarus*, *135*(2), 501–517.

Dritschel, D. G., & McIntyre, M. E. (2008). Multiple jets as PV staircases: The Phillips effect and the resilience of eddy-transport barriers. *Journal of the Atmospheric Sciences*, *65*(3), 855–874.

Dubos, T., Dubey, S., Tort, M., Mittal, R., Meurdesoif, Y., & Hourdin, F. (2015). DYNAMICO-1.0, an icosahedral hydrostatic dynamical core designed for consistency and versatility. *Geoscientific Model Development*, *8*(10), 3131–3150.

Ertel, H., & Rossby, C.-G. (1949). A new conservation-theorem of hydrodynamics. *Geofisica Pura e Applicata*, *14*(3–4), 189–193.

Espa, S., Lacorata, G., & Di Nitto, G. (2014). Anisotropic Lagrangian dispersion in rotating flows with a β effect. *Journal of Physical Oceanography*, *44*(2), 632–643.

Friedson, A. J., & Moses, J. I. (2012). General circulation and transport in Saturn's upper troposphere and stratosphere. *Icarus*, *218*(2), 861–875.

Friedson, A. J., West, R. A., Hronek, A. K., Larsen, N. A., & Dalal, N. (1999). Transport and mixing in Jupiter's stratosphere inferred from comet S-L9 dust migration. *Icarus*, *138*(1), 141–156.

Galperin, B., Hoemann, J., Espa, S., & Di Nitto, G. (2014). Anisotropic turbulence and Rossby waves in an easterly jet: An experimental study. *Geophysical Research Letters*, *41*, 6237–6243. https://doi.org/10.1002/2014GL060767

Galperin, B., Hoemann, J., Espa, S., Di Nitto, G., & Lacorata, G. (2016). Anisotropic macroturbulence and diffusion associated with a westward zonal jet: From laboratory to planetary atmospheres and oceans. *Physical Review E*, *94*(6), 063102.

Galperin, B., Hoemann, J., Espa, S., & Nitto, G. D. (2014). Anisotropic turbulence and Rossby waves in an easterly jet: An experimental study. *Geophysical Research Letters*, *41*, 6237–6243. https://doi.org/10.1002/2014GL060767

Galperin, B., Sukoriansky, S., & Dikovskaya, N. (2010). Geophysical flows with anisotropic turbulence and dispersive waves: flows with a β-effect. *Ocean Dynamics*, *60*(2), 427–441.

Galperin, B., Young, R. M. B., Sukoriansky, S., Dikovskaya, N., Read, P. L., Lancaster, A. J., & Armstrong, D. (2014). Cassini observations reveal a regime of zonostrophic macroturbulence on Jupiter. *Icarus*, *229*, 295–320.

Gargett, A., & Garner, T. (2008). Determining Thorpe scales from ship-lowered CTD density profiles. *Journal of Atmospheric and Oceanic Technology*, *25*(9), 1657–1670.

Gavrilov, N. M., Luce, H., Crochet, M., Dalaudier, F., & Fukao, S. (2005). Turbulence parameter estimations from high-resolution balloon temperature measurements of the MUTSI-2000 campaign. *Annales Geophysicae*, *23*(7), 2401–2413.

Gierasch, P. J., Conrath, B. J., & Read, P. L. (2004). Nonconservation of Ertel potential vorticity in hydrogen atmospheres. *Journal of the Atmospheric Sciences*, *61*(15), 1953–1965.

Guerlet, S., Spiga, A., Sylvestre, M., Indurain, M., Fouchet, T., Leconte, J., et al. (2014). Global climate modeling of Saturn's atmosphere. Part I: Evaluation of the radiative transfer model. *Icarus*, *238*, 110–124.

Ingersoll, A. P., & Pollard, D. (1982). Motion in the interiors and atmospheres of Jupiter and Saturn: Scale analysis, anelastic equations, barotropic stability criterion. *Icarus*, *52*(1), 62–80.

Kantha, L., & Hocking, W. (2011). Dissipation rates of turbulence kinetic energy in the free atmosphere: MST radar and radiosondes. *Journal of Atmospheric and Solar-Terrestrial Physics*, *73*(9), 1043–1051.

Kaspi, Y., Galanti, E., Hubbard, W. B., Stevenson, D. J., Bolton, S. J., Iess, L., et al. (2018). Jupiter's atmospheric jet streams extend thousands of kilometres deep. *Nature*, *555*(7695), 223–226.

Klymak, J. M., & Legg, S. M. (2010). A simple mixing scheme for models that resolve breaking internal waves. *Ocean Modelling*, *33*(3–4), 224–234.

Kraichnan, R. H. (1967). Inertial ranges in two dimensional turbulence. *Physics of Fluids*, *10*(7), 1417–1423.

Lacorata, G., & Espa, S. (2012). On the influence of a β-effect on Lagrangian diffusion. *Geophysical Research Letters*, *39*, L11605. https://doi.org/10.1029/2012GL05184

Marcus, P. S., & Lee, C. (1998). A model for eastward and westward jets in laboratory experiments and planetary atmospheres. *Physics of Fluids*, *10*(6), 1474–1489.

Marcus, P. S., & Shetty, S. (2011). Jupiter's zonal winds: Are they bands of homogenized potential vorticity organized as a monotonic staircase?. *Philosophical Transactions of the Royal Society A: Mathematical, Physical and Engineering Sciences*, *369*(1937), 771–795.

Pedlosky, J. (2013). *Geophysical fluid dynamics*: Springer Science & Business Media.

Phillips, N. A. (1956). The general circulation of the atmosphere: A numerical experiment. *Quarterly Journal of the Royal Meteorological Society*, *82*(352), 123–164.

Porco, C. C., West, R. A., McEwen, A., Del Genio, A. D., Ingersoll, A. P., Thomas, P., et al. (2003). Cassini imaging of Jupiter's atmosphere, satellites, and rings. *Science*, *299*(5612), 1541–1547.

Porco, C. C., West, R. A., Squyres, S., McEwen, A., Thomas, P., Murray, C. D., et al. (2004). Cassini imaging science: Instrument characteristics and anticipated scientific investigations at Saturn. *Space Science Reviews*, *115*, 363–497.

Read, P. L., Conrath, B. J., Fletcher, L. N., Gierasch, P. J., Simon-Miller, A. A., & Zuchowski, L. C. (2009). Mapping potential vorticity dynamics on Saturn: Zonal mean circulation from Cassini and Voyager data. *Planetary and Space Science*, *57*(14–15), 1682–1698.

Read, P. L., Gierasch, P. J., Conrath, B. J., Simon-Miller, A., Fouchet, T., & Yamazaki, Y. H. (2006). Mapping potential-vorticity dynamics on Jupiter. I: Zonal-mean circulation from Cassini and Voyager 1 data. *Quarterly Journal of the Royal Meteorological Society*, *132*(618), 1577–1603.

Read, P. L., Tabataba-Vakili, F., Wang, Y., Augier, P., Lindborg, E., Valeanu, A., & Young, R. M. B. (2018). Comparative terrestrial atmospheric circulation regimes in simplified global circulation models. Part II: Energy budgets and spectral transfers. *Quarterly Journal of the Royal Meteorological Society*, *144*(717), 2558–2576.

Rhines, P. B. (1975). Waves and turbulence on a beta-plane. *Journal of Fluid Mechanics*, *69*(03), 417–443.

Richardson, L. F. (1926). Atmospheric diffusion shown on a distance-neighbour graph. *Proceedings of the Royal Society of London. Series A, Containing Papers of a Mathematical and Physical Character*, *110*(756), 709–737.

Schneider, T., & Liu, J. (2009). Formation of jets and equatorial superrotation on Jupiter. *Journal of the Atmospheric Sciences*, *66*(3), 579–601.

Spiga, A., Guerlet, S., Millour, E., Indurain, M., Meurdesoif, Y., Cabanes, S., et al. (2020). Global climate modeling of Saturn's atmosphere. Part II: Multi-annual high-resolution dynamical simulations. *Icarus*, *335*, 113377.

Sukoriansky, S., Galperin, B., & Dikovskaya, N. (2002). Universal spectrum of two-dimensional turbulence on a rotating sphere and some basic features of atmospheric circulation on giant planets. *Physical Review Letters*, *89*(12), 124501.

Taylor, G. I. (1922). Diffusion by continuous movements. *Proceedings of the London Mathematical Society*, *2*(1), 196–212.

Thorpe, S. A. (2005). *The turbulent ocean*: Cambridge University Press.

Vallis, G. K. (2006). *Atmospheric and oceanic fluid dynamics: Fundamentals and large-scale circulation*: Cambridge University Press.

Vallis, G. K., & Maltrud, M. E. (1993). Generation of mean flows and jets on a beta plane and over topography. *Journal of Physical Oceanography*, *23*(7), 1346–1362.

Young, R. M. B., & Read, P. L. (2017). Forward and inverse kinetic energy cascades in Jupiter's turbulent weather layer. *Nature Physics*, *13*(11), 1135–1140.